Anomalous magnetic moment of the muon with dynamical QCD+QED

A. Westin[a]**, R. Horsley**[b]**, W. Kamleh**[a]**, Y. Nakamura**[c]**, H. Perlt**[d]**, P. E. L. Rakow**[e]**,
G. Schierholz**[f]** A. Schiller**[d]**, H. Stüben**[g]**, R. D. Young**[a]**, J. M. Zanotti**[*,a]

[a] *CSSM, Department of Physics, The University of Adelaide, Adelaide SA 5005, Australia*

[b] *School of Physics and Astronomy, University of Edinburgh, Edinburgh EH9 3FD, UK*

[c] *RIKEN Advanced Institute for Computational Science, Kobe, Hyogo 650-0047, Japan*

[d] *Institut für Theoretische Physik, Universität Leipzig, 04103 Leipzig, Germany*

[e] *Theoretical Physics Division, Department of Mathematical Sciences, University of Liverpool,
Liverpool L69 3BX, UK*

[f] *Deutsches Elektronen-Synchrotron DESY, 22603 Hamburg, Germany*

[g] *RRZ, Univeristy of Hamburg, 20146 Hamburg, Germany*

E-mail:
alex.westin@adelaide.edu.au,
james.zanotti@adelaide.edu.au

CSSM/QCDSF/UKQCD Collaboration

The current 3.5σ discrepancy between experimental and Standard Model determinations of the anomalous magnetic moment of the muon $a_\mu = (g-2)/2$ can only be extended to the discovery 5σ regime through a reduction of both experimental and theoretical uncertainties. On the theory side, this means a determination of the hadronic vacuum polarisation (HVP) contribution to better than 0.5%, a level of precision that demands the inclusion of QCD + QED effects to properly understand how the behaviour of quarks are modified when their electric charges are turned on. The QCDSF collaboration has generated an ensemble of configurations with dynamical QCD and QED fields with the specific aim of studying flavour breaking effects arising from differences in the quark masses and charges in physical quantities. Here we study these effects in a calculation of HVP around the SU(3) symmetric point. Furthermore, by performing partially-quenched simulations we are able to cover a larger range of quark masses and charges on these configurations and then fit the results to an SU(3) flavour breaking expansion. Subsequently, this allows for an extrapolation to the physical point.

[*]Speaker.

1. Introduction

There currently exists a $3.5 - 4$ standard deviation discrepancy between the experimentally measured anomalous magnetic moment of the muon, $a_\mu = \frac{g-2}{2}$, and current Standard Model predictions (see e.g. [1]). At present, the experimental [2] uncertainty and the total theoretical uncertainties are of comparable magnitude. The planned Muon $g - 2$ Experiment at Fermilab [3] aims to reduce the experimental uncertainty to 140 parts-ber-billion. Thus it is essential to get the theoretical uncertainties down to a comparable precision — this will require the "hadronic vacuum polarisation" (HVP) contributions to be known to better than 0.5%. Simulations of the QCD-only contribution to HVP have received a surge of interest over the past few years, with results now being quoted at the physical point with errors $\mathcal{O}(1\%)$. At this level of precision, contributions from QED effects are expected to play a role. In this talk, we present preliminary results for the electromagnetic contributions to the hadronic vacuum polarisation tensor — the key ingredient relevant to the QCD contribution to $(g - 2)_\mu$.

2. Accessing a_μ^{HVP}

We explore two methods of extracting the HVP contribution to the anomalous magnetic moment from the lattice. First we will take a more traditional approach where we determine the vacuum polarisation from the vacuum polarisation tensor, $\Pi_{\mu\nu}(Q)$, as first described in [4, 5]. Secondly we will investigate the time-momentum representation method proposed in [6] to extract a value for a_μ^{HVP}.

2.1 Vacuum polarisation tensor

We can calculate a_μ^{HVP} from the vacuum polarisation function $\Pi(Q^2)$ using

$$a_\mu^{HVP} = 4\alpha^2 \int_0^\infty dQ^2 K(Q^2; m_\mu^2) \left\{ \Pi(Q^2) - \Pi(0) \right\}, \tag{2.1}$$

where $K(Q^2; m_\mu^2)$ is a known kernel function [4], and the polarisation function $\Pi(Q^2)$ is determined from the polarisation tensor

$$\Pi_{\mu\nu} = \int d^4x e^{iQ\cdot x} \langle J_\mu(x) J_\nu(0) \rangle = \left(Q_\mu Q_\nu - \delta_{\mu\nu} Q^2 \right) \Pi\left(Q^2\right). \tag{2.2}$$

2.2 Time-moment representation

In the time-moment representation (TMR), the vacuum subtracted polarisation function, $\hat{\Pi}(Q^2) \equiv 4\pi^2 \left(\Pi(Q^2) - \Pi(0) \right)$, is obtained from the spatially summed two-point correlator, $G(t)$,

$$\hat{\Pi}(Q^2) = 4\pi^2 \int_0^\infty dt\, G(t) \left(t^2 - \frac{4}{Q^2} \sin^2\left(\frac{Qt}{2} \right) \right), \tag{2.3}$$

$$G(t) = - \int d^3x \langle J_i(x) J_i(0) \rangle. \tag{2.4}$$

Substituting this into Eq. (2.1), one finds

$$a_\mu^{HVP} = \left(\frac{\alpha}{\pi} \right)^2 \int_0^\infty dt\, G(t) \tilde{K}(t; m_\mu), \tag{2.5}$$

where we employ the analytic form for $\tilde{K}(t; m_\mu)$ derived in [7].

3. Simulation details

We follow the flavour-breaking program outlined in [8, 9] originally for QCD, and extended to include electromagnetic interactions in [10, 11]. Starting from the symmetric point $m_u = m_d = m_s$, our strategy is to keep the singlet quark mass $\bar{m} = (m_u + m_d + m_s)/3$ fixed at its physical value while $\delta m_q \equiv m_q - \bar{m}$ is varied. This procedure leads to highly constrained polynomials in δm_q and e_q^2, and thus reduces the number of free parameters drastically.

For the partially-quenched, flavour-diagonal $a\bar{a}$ ($a = u, d, s$) octet (vector) meson masses, with all annihilation channels turned off, a group theoretical analysis incorporating both QCD and QED terms leads to the mass formula to leading order in α_{EM} and second order in δm_q

$$
\begin{aligned}
M(a\bar{a}) =& M_0 + 2\alpha\delta\mu_a + \beta_0 \frac{1}{6}(\delta m_u^2 + \delta m_d^2 + \delta m_s^2) + 2\beta_1\delta\mu_a^2 + \beta_0^{EM}(e_u^2 + e_d^2 + e_s^2) \\
&+ 2\beta_1^{EM}e_a^2 + \gamma_0^{EM}(e_u^2\delta m_u + e_d^2\delta m_d + e_s^2\delta m_s) + 2\gamma_1^{EM}e_a^2\delta\mu_a \\
&+ 2\gamma_4^{EM}(e_u^2 + e_d^2 + e_s^2)\delta\mu_a + 2\gamma_5^{EM}e_a(e_u\delta m_u + e_d\delta m_d + e_s\delta m_s) \,.
\end{aligned}
\tag{3.1}
$$

We have distinguished between sea (m_q) and valence (partially-quenched, PQ) quark masses μ_a with $\delta\mu_a = \mu_a - \bar{m}$.

The introduction of quark charges complicates the definition of an SU(3) symmetric point. In [10] we introduced the Dashen scheme which absorbs all electromagnetic effects in the neutral, purely connected pseudoscalar mesons ($m_\pi^{a\bar{a}}$) into the definition of the quark mass, which we refer to as the "Dashen mass" μ_a^D. This drastically simplifies the flavour-breaking expansions of the pseudoscalar mesons [10], while the effect on the expansion of the vector mesons as needed here is to replace $\delta\mu_a$ in Eq. (3.1) with $\delta\mu_a^D$. A natural definition for the SU(3) symmetric point in this scheme is then one where $m_\pi^{u\bar{u}} = m_\pi^{d\bar{d}} = m_\pi^{s\bar{s}}$. This tuning was performed on two volumes in [10].

We employ five ensembles of fully dynamical QCD+QED lattice configurations generated by the QCDSF collaboration, including simulations on two different volumes, $32^3 \times 64$, and $48^3 \times 96$, with lattice spacing $a = 0.068(1)$fm, and an exaggerated QED coupling $\alpha_{\text{EM}} \sim 0.1$. Our simulation set-up employs the so-called QED_L formulation [12], where the zero mode of the photon field is removed on each time slice for the valence quarks. However, since in this work we only consider electrically neutral $q\bar{q}$ hadronic systems, photon zero modes are in any case unlikely to have any effect.

The details of the five ensembles are summarised in Table 1 where we provide the masses of the unitary neutral and charged pseudoscalar mesons. In order to better constrain the coefficients of the flavour-breaking expansions, on each ensemble we employ partially-quenched quark masses corresponding to neutral pseudoscalar meson masses in the range $260 \leq m_{q\bar{q}} \leq 770$ MeV. Quark charges are also partially quenched in that we allow for charges $Q_q \in \left(0, -\frac{1}{3\sqrt{13}}, +\frac{2}{3\sqrt{13}}, \pm\frac{1}{3}, \pm\frac{\sqrt{2}}{3}, \pm\frac{2}{3}\right)e$. At our enhanced QED coupling ($e \approx \sqrt{13.7}\,e^{\text{phys}}$), the quark charges $Q_q = \left(-\frac{1}{3\sqrt{13}}, +\frac{2}{3\sqrt{13}}\right)e$ allow for simulations to be performed with near-physical valence quark charges.

As first observed in [13], we find a clear charge dependence of the vector current renormalisation constant, Z_V. This will be discussed in more detail in a forthcoming publication.

2

Ensemble	$L^3 \times T$	N_f	$m_{u\bar{u}}$	$m_{d\bar{d}}$	$m_{s\bar{s}}$	$m_{q\bar{q}}^{min}L$	m_{π^+}	m_{K^+}
1	$32^3 \times 64$	2+1	430	405	405	4.4	435	435
2	$32^3 \times 64$	2+1	360	435	435	4.0	415	415
3	$32^3 \times 64$	1+1+1	290	300	570	3.2	320	470
4	$48^3 \times 96$	2+1	430	405	405	6.7	435	435
5	$48^3 \times 96$	2+1	360	435	435	5.9	420	420

Table 1: Ensembles used in this work. All masses are in MeV.

4. Results and discussion

4.1 Finite Volume Effects

When working on a finite four-torus with dimensions $L^3 \times T$, the single polarisation function in Eq. (2.2), as valid for $O(4)$, is replaced by five independent functions corresponding to the five irreducible representations of the finite cubic symmetry group $H(3)$ [6, 14]

$$
\begin{aligned}
A_1 &: \sum_i \bar{\Pi}_{ii} = \left(3q^2 - \vec{q}^2\right) \bar{\Pi}_{A_1}, \quad & T_1 &: \bar{\Pi}_{4i} = -(q_4 q_i) \bar{\Pi}_{T_1} \\
A_1^{44} &: \bar{\Pi}_{44} = \left(\vec{q}^2\right) \bar{\Pi}_{A_1^{44}}, \quad & T_2 &: \bar{\Pi}_{ij} = -(q_i q_j) \bar{\Pi}_{T_2}, i \neq j, \\
& & E &: \bar{\Pi}_{ii} - \sum_i \bar{\Pi}_{ii}/3 = \left(-q_i^2 + \vec{q}^2/3\right) \bar{\Pi}_E.
\end{aligned}
\tag{4.1}
$$

These five functions should agree in the infinite volume and continuum limits, hence we are provided with a method for investigating the impact of the finite volume on our results. In left plot of Fig. 1, we display the A_1, A_1^{44}, E, T_1 polarisation functions obtained from the $32^3 \times 64$ volume close to the SU(3) symmetric point (i.e. ensemble 1 in Table 1). Here we observe a clear discrepancy between the irreducible representations of the vacuum polarisation tensor and indicates the presence of finite volume effects in the simulations.

This behaviour is carried through to a_μ^{HVP} after we follow the procedure outlined in Sec. 2.1. This is seen by the scatter of the data points displayed in the right plot of Fig. 1 for the $32^3 \times 64$ volume. When we repeat the process for the larger $48^3 \times 96$ volume at the same quark masses (ensemble 2), we observe a pronounced reduction in the scatter of results obtained from the different irreducible representations. This provides us with confidence that results obtained on the larger volume have only a small remnant finite size effect.

4.2 Time Moment

We will now turn our attention to determining a_μ^{HVP} from the time moment representation as given in Eq. (2.5), following the method proposed in [7]. At large times, the 2 point function $G(t)$ suffers from a loss of signal into statistical noise and is contaminated by the backwards propagating state. Since Eq. (2.5) requires $G(t)$ to be known to infinite times, this issue is overcome by only using the 2 point function data, $G^{\text{data}}(t)$ up to some value of $t = t_{cut}$. After this time, we fit a single exponential with the ground state vector meson mass, E_0, such that

$$
G(t) = \begin{cases} G^{\text{data}}(t) & t \leq t_{cut}, \\ A e^{-E_0 t} & t > t_{cut}. \end{cases}
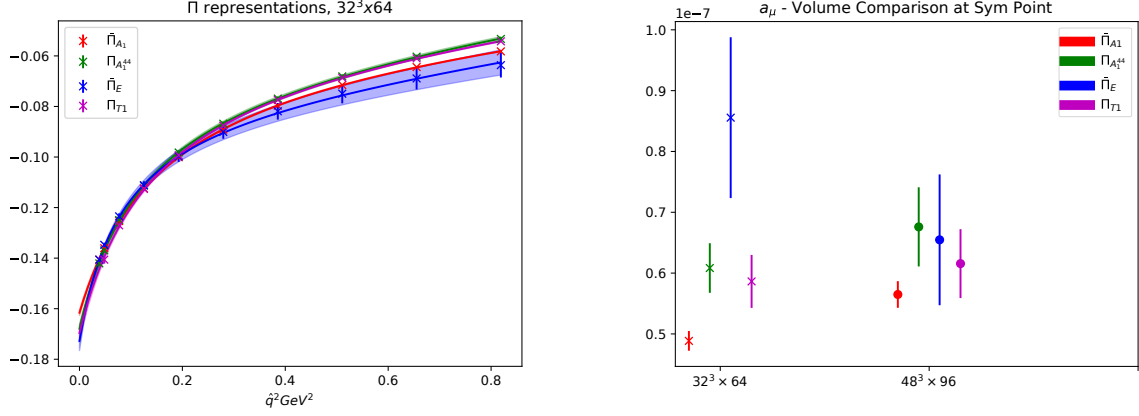\tag{4.2}
$$

Figure 1: Left: Polarisation functions from the A_1, A_1^{44}, E, T_1 irreducible representations from the $32^3 \times 64$, ensemble 1. Right: a_μ^{HVP} determined via the vacuum polarisation functions belonging to the different irreducible representations of the finite volume for two volumes (ensembles 1 and 2).

For the region $t < t_{cut}$ we use a cubic spline over the lattice data before computing the contribution of this region to the integral in Eq. (2.5). We choose t_{cut} such that the single exponential ansatz matches the data before the signal is lost to noise, and that it forms a smooth continuous line with the spline of that data at t_{cut}. An example for $t_{cut} = 26$ on ensemble 1 is shown in Fig. 2a.
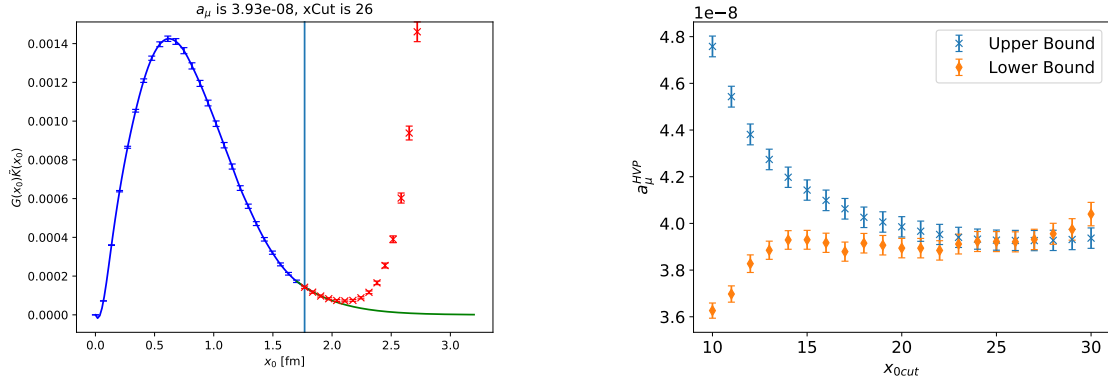
(a) Blue points are correlator data used in constraining a cubic spline (blue curve). Red crosses are correlator data after the t_{cut} (vertical line), which are ignored. Green line in the tail is from our exponential function for $t > t_{cut}$ region.

(b) Bounding method [15]. Upper and lower bounds agree around the $t = 26$ mark, which verifies our choice of $t_{cut} = 26$ for this particular correlator.

Figure 2

We can check our choice of t_{cut} using the recent bounding method [15, 16]. For this we define $G(t)$ as

$$G(t) = \begin{cases} G^{\text{data}}(t) & t \le t_{cut}, \\ G^{\text{data}}(t_{cut})e^{-E(t-t_{cut})} & t > t_{cut}, \end{cases} \qquad (4.3)$$

where we have an upper bound from $E = E_0$ and a lower bound from $E = \log\left[\frac{G(t_{cut})}{G(t_{cut}+1)}\right]$. When these two bounds agree, we find the optimal choice for t_{cut}.

In Fig. 2b we see that the upper and lower bounds converge at $t_{cut} = 26$, which matches with when our exponential fit matches on smoothly with $G(t)$ in Fig. 2a.

We note that this procedure can easily be improved by including states beyond the ground state, allowing for smaller values of t_{cut} to be used [15, 16]. This will be pursued in future work.

The above bounding method is then repeated for all partially quenched quarks on all five ensembles in Table 1. We can then calculate a_μ^{HVP} on each of our ensembles. These are plotted against the Dashen mass in Fig. 3 for $32^3 \times 64$ (left) and $48^3 \times 96$ (right) volumes. Recalling the flavour-breaking expansion for the flavour-diagonal vector mesons given in Eq. (3.1), then since the SU(3)-flavour properties of a_μ^{HVP} are the same, we can apply the same expansion for a_μ^{HVP} to extrapolate to the physical masses.

Figure 3 shows our values for a_μ^{HVP} plotted against Dashen mass, μ_q^D. Note that for ease of plotting, we have compressed the direction relevant to the variation of a_μ^{HVP} with sea quark mass by shifting all points to the physical sea quark masses $\delta m_q = \delta m_q^{phys}$. The physical values for the valence quark masses are given by the red (up), green (down) and blue (strange) vertical dashed lines. The final value for a_μ^{HVP} is obtained by taking the appropriate charge-weighted combination of all three quark flavour contributions at their physical masses. As this work is still preliminary, we refrain from quoting numbers at this stage, however by comparing the results between the volumes it is obvious that there are significant finite volume effects, particularly in the $32^3 \times 64$ volume. Given the analysis presented in Sec. 4.1, this is not surprising.

Finally, we note that the results from both volumes are described well by the flavour-breaking expansions of Eq. (3.1) and that our use of partially-quenched valence quarks covering a large range of masses and electric charges allows for contraints to be placed on the various parameters. In particular, we note the small difference in slopes between the red (up quarks with charge $+2/3e$) and green (down/strange quarks with charge $-1/3e$) curves which is a purely electromagnetic effect. In future work we hope to improve the quality of the data and range of ensembles available in order to isolate the contribution from the QED terms.
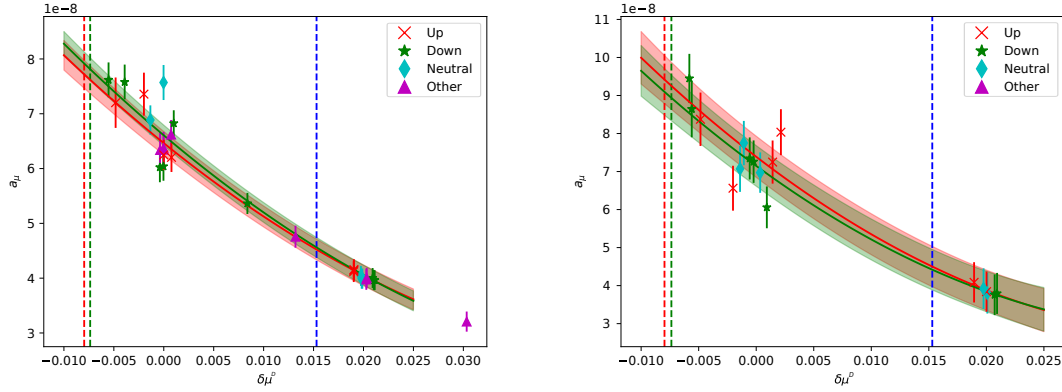
Acknowledgements

Figure 3: a_μ^{HVP} against Dashen mass, *left*: $32^3 \times 64$, *right*: $48^3 \times 96$. Note that points are shifted to $\delta m = \delta m^{phys}$ line. Colours refer to quarks with different charges, *red*: Up quark, *green*: Down/strange quarks, *cyan*: 'Neutral' quark, *magenta*: other charges.

References

[1] A. Keshavarzi, D. Nomura and T. Teubner, `1802.02995`.

[2] MUON G-2 collaboration, G. W. Bennett et al., *Phys. Rev.* **D73** (2006) 072003 [`hep-ex/0602035`].

[3] MUON G-2 collaboration, A. Chapelain, *EPJ Web Conf.* **137** (2017) 08001 [`1701.02807`].

[4] T. Blum, *Phys. Rev. Lett.* **91** (2003) 052001 [`hep-lat/0212018`].

[5] QCDSF collaboration, M. Göckeler et al., *Nucl. Phys.* **B688** (2004) 135 [`hep-lat/0312032`].

[6] D. Bernecker and H. B. Meyer, *Eur. Phys. J.* **A47** (2011) 148 [`1107.4388`].

[7] M. Della Morte et al., *JHEP* **10** (2017) 020 [`1705.01775`].

[8] W. Bietenholz et al., *Phys. Lett.* **B690** (2010) 436 [`1003.1114`].

[9] W. Bietenholz et al., *Phys. Rev.* **D84** (2011) 054509 [`1102.5300`].

[10] R. Horsley et al., *JHEP* **04** (2016) 093 [`1509.00799`].

[11] R. Horsley et al., *J. Phys.* **G43** (2016) 10LT02 [`1508.06401`].

[12] M. Hayakawa and S. Uno, *Prog. Theor. Phys.* **120** (2008) 413 [`0804.2044`].

[13] P. Boyle et al., *JHEP* **09** (2017) 153 [`1706.05293`].

[14] C. Aubin et al., *Phys. Rev.* **D93** (2016) 054508 [`1512.07555`].

[15] S. Borsanyi et al., *Phys. Rev.* **D96** (2017) 074507 [`1612.02364`].

[16] RBC, UKQCD collaboration, T. Blum et al., *Phys. Rev. Lett.* **121** (2018) 022003 [`1801.07224`].

[17] T. R. Haar, Y. Nakamura and H. Stüben, *EPJ Web Conf.* **175** (2018) 14011 [`1711.03836`].

[18] SCIDAC, LHPC, UKQCD collaboration, R. G. Edwards and B. Joo, *Nucl. Phys. Proc. Suppl.* **140** (2005) 832 [`hep-lat/0409003`].